Propagating Stress Waves During Epithelial Expansion

Shiladitya Banerjee,[1*,†] Kazage J. C. Utuje,[2] and M. Cristina Marchetti[2,3*,‡]
[1]James Franck Institute, The University of Chicago, Chicago, Illinois 60637, USA
[2]Department of Physics, Syracuse University, Syracuse, New York 13244, USA
[3]Syracuse Biomaterials Institute, Syracuse University, Syracuse, New York 13244, USA
(Received 8 November 2014; published 2 June 2015)

Coordinated motion of cell monolayers during epithelial wound healing and tissue morphogenesis involves mechanical stress generation. Here we propose a model for the dynamics of epithelial expansion that couples mechanical deformations in the tissue to contractile activity and polarization in the cells. A new ingredient of our model is a feedback between local strain, polarization, and contractility that naturally yields a mechanism for viscoelasticity and effective inertia in the cell monolayer. Using a combination of analytical and numerical techniques, we demonstrate that our model quantitatively reproduces many experimental findings [Nat. Phys. 8, 628 (2012)], including the buildup of intercellular stresses, and the existence of traveling mechanical waves guiding the oscillatory monolayer expansion.

DOI: 10.1103/PhysRevLett.114.228101 PACS numbers: 87.10.Ca, 87.18.Fx, 87.18.Gh

Many developmental processes, such as embryogenesis [1], tissue morphogenesis [2], wound healing [3], and cancer metastasis [4], involve collective cell migration [5] and long-scale force generation, which in turn rely on the interplay of cell-cell cohesion, cell adhesion to the extracellular matrix, as well as myosin based contractility [6,7]. Recent experiments reveal that unconstrained tissue expansion is accompanied by propagating mechanical waves and buildup of intercellular stresses [8]. These waves are controlled by expressions of myosin activity, cell-cell adhesion, and cytoskeletal remodeling. These findings pose a fundamental physical question: how do waves arise in overdamped active elastic media? What are the underlying spatiotemporal patterns governing stress propagation in dense expanding cell layers?

Active materials encompass a wide range of living and nonliving systems with inborn mechanical stresses regulated by chemical reactions. Generic descriptions of the dynamics of such materials predict a broad class of nonequilibrium states including spontaneous flow, wave propagation, and pattern formation [9–12]. While the dynamics of active fluids have been extensively studied, quantitative descriptions of active contractile materials are much less developed. Recent work has suggested that a polarized elastic medium driven by chemical agents can exhibit fingerlike protrusions and internal stress accumulation during expansion [13,14]. It remains unclear, however, how cell contractility, polarization, or tissue cohesion influence stress generation and wave propagation. Earlier work by two of us and others showed that the coupling of mechanical and chemical degrees of freedom can lead to an effective inertia and sustained propagation of waves [15–17]. Related models also emphasize that turnovers in actomyosin activity are essential to capture spontaneous oscillations in cell cytoskeleton [18,19]. In this Letter, we propose a new mechanism of stress propagation in multicellular materials based on a local feedback between elastic deformations and cell contractility.

We consider a minimal model for an expanding cell monolayer, described as an elastic continuum coupled to an internal degree of freedom, the concentration of active contractile units. The assumption of elasticity is supported by experimental evidence that in cohesive cell layers stress and strain tend to be in phase, as in elastic materials [7,8]. The contractile units represent actomyosin assemblies that locally generate contractile stresses in the cells. We propose that tissue expansion promotes the rate of assembly of these contractile units, leading to larger contractile forces that can compete with propulsion forces. This mechanochemical feedback successfully captures the experimentally observed stress waves [8]. The steady state of such a system is described by polarization being largest at the edges and lowest at the center. A scaling model for the expanding cell layer captures the mechanical oscillations and predicts self-sustained periods of stiffening and fluidization in the tissue.

Continuum model for the spreading cell layer.—We consider a thin film of cell monolayer spreading in the x-y plane, with height $h(t)$ and length $L(t)$ at time t [Fig. 1(a), inset]. In the absence of external forces, in-plane force-balance gives $\partial_j \Sigma_{ij} + \partial_z \Sigma_{iz} = 0$, where Σ is the stress tensor and the latin indices denote in-plane coordinates x, y. For $h \ll L, d$, the x and y linear extensions of the cell layer, we average the force-balance equation across the z direction to obtain $h\partial_j \sigma_{ij} = \Sigma_{iz}|_{z=0}$, where $\boldsymbol{\sigma}(x,y) = \frac{1}{h}\int_0^h dz \Sigma(x,y,z)$, assuming that the top layer ($z = h$) is stress free. The shear stress at the cell-substrate interface is the traction stress exerted by the cell on the substrate. It is given by $\Sigma_{iz}|_{z=0} = T_i = \Gamma \partial_t u_i - f_0 p_i$, with Γ the friction density, $\mathbf{u}$ the elastic displacement field, $\mathbf{p}$ the cell

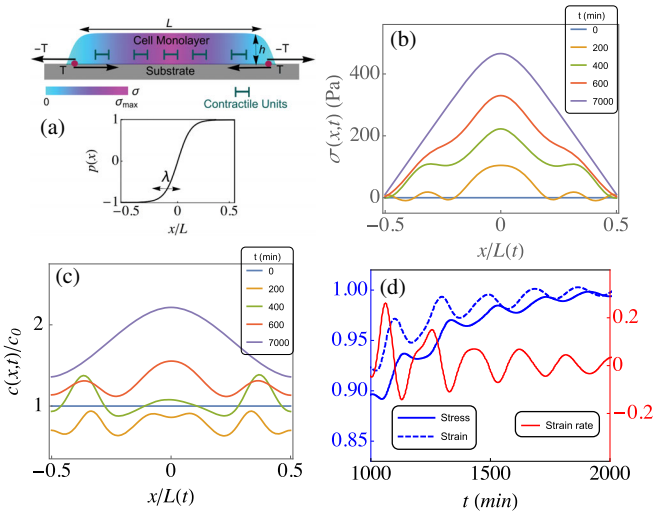

FIG. 1 (color online). (a) Top: Schematic of a spreading cell monolayer. Traction stresses (**T**) are indicated by arrows and the color map denotes local magnitude of monolayer stress. Bottom: Profile of cell polarization. (b) Time evolution of the internal stress $\sigma(x,t)$ in the monolayer. (c) Time evolution of the concentration of contractile units, c, normalized by its equilibrium value. (d) Midline stress $\sigma(0,t)/\sigma_\infty(0,t)$ (blue solid line), midline strain $\varepsilon(0,t)/\varepsilon_\infty(0,t)$ (blue dashed line), and midline strain rate $\dot{\varepsilon}(0,t)$ (red solid line, units on right axis 10^{-4} s^{-1}) as functions of time. Parameters: $B = 120$ Pa, $\beta = 200$ Pa, $\Pi/\beta = 10^{-3}$, $\tau = 350$ min, $\alpha/c_0 = 1/560$ min^{-1}, $L_0 = 600$ μm, $h_0 = 6$ μm, $f_0 = 4$ Pa, $\lambda = 30$ μm, $\Gamma = 0.009$ nN min$/\mu$m^3, $D = 26$ μm^2/ min.

polarization, and f_0 the propulsion force per unit cross-sectional area. The term $f_0 p_i$ is supported by the experimental observation that the local velocity of expanding monolayers is generally not aligned with traction, requiring the existence of an internally generated driving force associated with cell motility [20]. Both Γ and f_0 are controlled by integrin-mediated cell-environment interactions. We further simplify the model by assuming translational invariance along the y direction. The equation of motion governing the displacement field, $u(x,t)$, of the cell layer is $(0 < |x| < L/2)$,

$$\Gamma \partial_t u = f_0 p(x,t) + h(t)\partial_x \sigma, \tag{1}$$

where $\sigma(x,t)$ is the internal stress in the monolayer, $\sigma = -\Pi + B\varepsilon + \sigma_a(c)$. It is given by the sum of an internal pressure (Π), an elastic stress, with B the compressional elastic modulus and $\varepsilon = \partial_x u$ the strain field, and an active stress σ_a that depends on the concentration c of active contractile units, such as phosphorylated myosins interacting with actin filaments. The constant pressure Π accounts for internal growth due to cell proliferation which is assumed negligible without loss of generality. The active stress is proportional to the chemical potential of the active species μ, which we take proportional to the logarithm of the concentration of the species. We thus have $\sigma_a(c) = \beta \log(c/c_0)$, where c_0 is the concentration of contractile elements in equilibrium ($f_0 = 0$) and $\beta > 0$ the magnitude of the contractile stress. The dynamics of the concentration field $c(x,t)$ is given by

$$\partial_t c = -\frac{1}{\tau}(c - c_0) + \alpha\varepsilon - \partial_x J, \tag{2}$$

where τ is the time scale of turnover of the contractile elements, $\alpha > 0$ is the rate of production of c due to local extension (or degradation due to contraction), and $J(x,t)$ is the current responsible for transport of these active units. This is in contrast to our earlier works [15,16], where the strain field enters the dynamics of c through the decay rate. The total current is a sum of diffusive and convective fluxes, $J = -D\partial_x c + c\partial_t u$, where D is an effective diffusion constant, describing the tendency of neighboring cells to equalize activity levels. Together, Eqs. (1) and (2) define the dynamics of the spreading monolayer, given the form of $p(x,t)$, the boundary and initial conditions. We first consider the case of constant but nonuniform propulsion force given by $p(x,t) = \tanh(x/\lambda)$, where λ is a length scale controlling the width of the transition zone from left-moving to right-moving cells at the center of the monolayer [see Fig. 1(a)]. The length of the spreading layer at time t is given by, $L(t) = L_0 + u(L_0/2,t) - u(-L_0/2,t)$, and the height is determined by the condition of volume conservation, $h(t) = h_0 L_0/L(t)$, with L_0 and h_0 the initial length and height of the monolayer, respectively. The boundary of the monolayer is stress free, i.e., $\sigma(\pm L/2,t) = 0$ at all times. We assume that the monolayer is initially undeformed, $u(x,0) = 0$, with an equilibrium concentration of contractile elements, $c(x,0) = c_0$, and choose a no-flux boundary condition for c, $\partial_x c(\pm L/2,t) = 0$.

Propagating waves.—In the absence of propulsion force ($f_0 = 0$), the cell layer is in a quiescent homogeneous state, with $u = 0$ and $c = c_0$. When $f_0 \neq 0$, the cell layer spreads and reaches a steady state at long times. We have integrated numerically Eqs. (1), (2) with the given initial and boundary conditions, using the Runge-Kutta-Fehlberg method. The model parameters are chosen to quantitatively describe the available experimental data for MDCK colonies [8,21]. The phase diagram shown in Fig. 2(a) displays three dynamical regimes in terms of contractile activity β and compressional modulus B (controlled by cell-cell adhesion): a region where fluctuations are stable and diffusive at low contractility, an intermediate region where the system supports propagating waves, and a region where the propagating waves become unstable at high contractility. There is good agreement between the boundaries obtained via numerical solution of the full nonlinear equations (red squares) and those determined by the linear instability of fluctuations about the equilibrium, undeformed state [21] and about the long-time solution of the mean-field model in Eqs. (4). In the region of

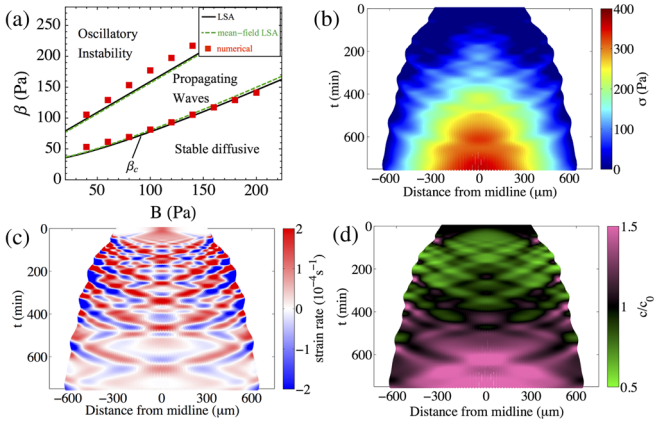

FIG. 2 (color online). (a) Phase diagram of the spreading gel. The vertical axis represents the contractile activity β and the horizontal axis is the compressional modulus B. Three behaviors are observed: stable diffusive, stable propagating waves, and oscillatory instability. The red squares are obtained from the numerical solutions of the full nonlinear model, the black solid lines are the results of the linear stability analysis (LSA) of the equilibrium state (at $q = 13.5/L_0$) [21], and the dashed green lines refer to the LSA of the mean-field model given in Eqs. (4). Kymographs of (b) the monolayer stress field, (c) strain rate $\partial_t \varepsilon(x,t)$, and (d) $c(x,t)/c_0$. The parameter values are taken to be the same as in Fig. 1.

propagating waves, the stress initially shows a few local maxima [Fig. 1(b)], which evolve towards a single maximum at the center of the monolayer, as observed in experiments [8,22]. The concentration of contractile elements also oscillates and builds up at the center of the monolayer [Fig. 1(c)]. The stress waves propagate nearly in phase with the strain field, whereas the strain rate fluctuates nearly out of phase with the stress [Fig. 1(d)]. Thus, the response of the material is dominated by elastic relaxation with dissipation induced by turnovers in contractility on a time scale τ. The waves span the entire length of the monolayer and consist of a strain rate wave front that propagates inwards from the edge, and then travels back to the edge, resembling an X pattern, as observed experimentally [8]. With the given parameter values our numerical simulations capture the mechanical waves as evident in the kymographs of stress, strain rate, and concentration of contractile units [Figs. 2(b)–(d)].

To understand the origin of wave propagation and estimate the wave frequency, it is useful to examine the linear fluctuations in the strain field $\delta\varepsilon$ and the concentration field δc, about the quiescent homogeneous state $u = 0$, $c = c_0$, and no spreading force. Using Eqs. (1) and (2), one can then eliminate δc from such linearized equations to obtain the linearized dynamics of strain fluctuations,

$$\tau\Gamma\partial_t^2\delta\varepsilon + \Gamma\partial_t\delta\varepsilon = h_0(B_{\rm eff} + \eta_{\rm eff}\partial_t - \tau BD\partial_x^2)\partial_x^2\delta\varepsilon, \quad (3)$$

The above equation shows that the coupling of strain to concentration field yields an effective mass density (inertia), $\tau\Gamma$, and viscoelasticity characterized by an effective elastic modulus, $B_{\rm eff} = B + \alpha\beta\tau/c_0$, and an effective viscosity $\eta_{\rm eff} = (B - \beta + D\Gamma/h_0)\tau$. The dynamics of strain fluctuations resembles a damped Kelvin-Voigt oscillator with a characteristic frequency of oscillations, $\omega_0 = q\sqrt{h_0(B_{\rm eff} + \tau q^2 BD)/(\tau\Gamma)}$, with q the wave vector. The estimate for the time period $2\pi/\omega_0$ agrees well with the time period determined from numerics for $q \simeq 4\pi/L_0$ [see Fig. 3(a)] and with the value measured in recent experiments [8]. Finally, we note that if the concentration c is conserved ($\tau \to \infty$; $\alpha = 0$), stable propagating waves are spontaneously generated for $0 < B - \beta + D\Gamma/h_0 < 2\sqrt{DB\Gamma/h_0}$. If diffusion is slow compared to elastic relaxation, $D\Gamma/Bh_0 \ll 1$, stable propagating waves are not observed [21]. In the opposite limit of infinitely fast turnovers in contractility ($\tau \to 0$), strain fluctuations decay diffusively at a rate $\simeq Bh_0/\Gamma L^2$.

Mean field model.—The mean field limit of the continuum model is obtained by neglecting spatial variations in c and ε and it is formulated in terms of the length (L), height (h), and the average concentration of contractile elements, $\bar{c}(t) = (1/L)\int_0^L dx c(x,t)$, with

$$\gamma\frac{dL}{dt} = F_0 - A(t)\sigma(t), \quad (4a)$$

$$\frac{d\bar{c}}{dt} + \frac{\bar{c}}{L}\frac{dL}{dt} = -\frac{1}{\tau}(\bar{c} - c_0) + \alpha\varepsilon, \quad (4b)$$

with F_0 the propulsion force, γ the friction, $A(t) = dh(t)$ the cross-sectional area, $\varepsilon(t) = L(t)/L_0 - 1$ the strain, and $\sigma(t)$ the internal stress given by $\sigma(t) = B\varepsilon(t) + \beta[\bar{c}(t)/c_0 - 1]$. The height is determined using the incompressibility condition, with the size in the y direction, d, fixed. The steady state solution is $L_\infty = L_0/(1-\Lambda)$, $h_\infty = h_0(1-\Lambda)$ and $c_\infty = c_0 + \alpha\tau\Lambda/(1-\Lambda)$, with $\Lambda = c_0 F_0/dh_0(Bc_0 + \alpha\beta\tau)$ the net compressive strain in the z direction. For a given value of elastic modulus B, the mean-field model predicts oscillatory solutions for $\beta > \beta_c$, where $\beta_c(B)$ defines the phase boundary in (B,β) plane separating the regions of propagating waves and diffusive spreading [dashed line in Fig. 2(a)]. For $\beta < \beta_c$ the monolayer diffusively approaches the steady state (c_∞, L_∞). This simple mean-field approach allows us to study the material response of the monolayer characterized by an effective elastic modulus, $B_{\rm MF} = d\sigma/d\varepsilon$. The oscillatory regime ($\beta > \beta_c$) exhibits sustained oscillations in the material rigidity, $B_{\rm MF}$, with a slow period of stiffening followed by a sharp turnover [see Fig. 3(b)]. For $\beta < \beta_c$, the material gradually stiffens with $B_{\rm MF}$ asymptotically approaching the value $B_{\rm eff}$. These oscillations reflect self-sustained turnovers in the cytoskeleton with periodic reinforcement and fluidization on different time scales, which was invoked to

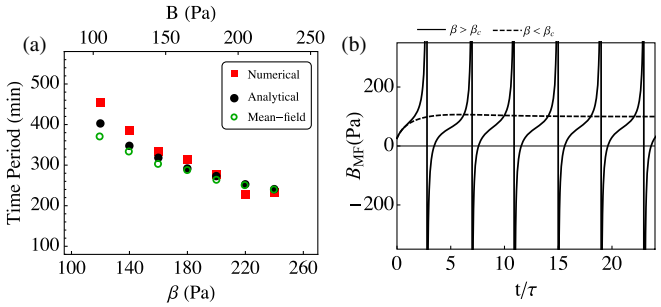

FIG. 3 (color online). (a) Period of oscillation determined from the numerical solution to Eqs. (1) and (2) (red squares), obtained from Eq. (3) (black solid circles), and as predicted by the mean-field model (green open circles) for various β and B. (b) Mean-field elastic modulus B_{MF} of the cell monolayer as a function of time, showing oscillatory stiffening or fluidization for $\beta = 100$ Pa (solid) and steady stiffening for $\beta = 30$ Pa (dashed). Parameters: $B = 60$ Pa, $\tau = 350$ min, $c_0/\alpha = 780$ min, $F_0 = 8$ nN, $\gamma = 9$ nN min $/\mu$m, $dh_0/L_0^2 = 0.1$.

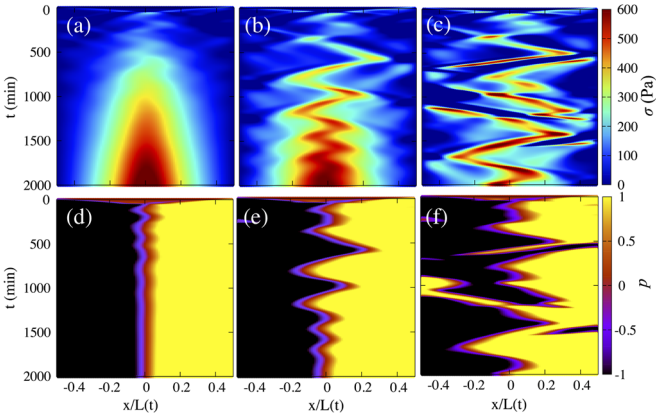

FIG. 4 (color online). Spatiotemporal evolution of internal stress (a)–(c) and polarization (d)–(f) as the polarization induced tension β' is increased (left to right). (a),(d) X waves, $\beta' = 12$ nN$/\mu$m; (b),(e) traveling stress pulse, $\beta' = 17$ nN$/\mu$m; (c),(f) complex oscillatory patterns, $\beta' = 24$ nN$/\mu$m. Parameters: $w = 4.3$ μm$/$ min, $w' = 0.21$ μm$/$ min, $\kappa = 193$ μm$^2/$ min, $a = 0.07$ min^{-1}, $b = 0.03$ min^{-1}. Other parameter values are the same as in Fig. 1. See Supplemental Material [21] for kymographs of strain rate, velocity and traction stress.

be the underlying mechanism of wave propagation in Ref. [8].

Time-dependent propulsion forces.—Finally, we consider time variations of the propulsion force, as arising from the dynamics of cell polarization $p(x,t)$ given by

$$\partial_t p = (a - bp^2)p + \kappa\partial_x^2 p - w\partial_x\varepsilon + w'\partial_x(c/c_0), \quad (5)$$

where the first two terms with $b > 0$ allow for the onset of a homogeneous polarized state when $a > 0$. The stiffness constant κ characterizes the cost of local deformations in the polarization. The last two terms in Eq. (5) define active couplings of p to the strain and the concentration field, with $w, w' > 0$, such that p aligns with the gradient of monolayer density and the concentration field. In other words, cell polarization is enhanced in the direction opposite to that of elastic restoring forces. Additionally, polarization gradients can induce mechanical stresses, and the stress tensor is modified to read $\sigma = B\varepsilon + \sigma_a(c) + \beta'\partial_x p$, where $\beta' > 0$ is a contractile tension induced by polarization gradients. We assume a no-flux boundary condition $p'(\pm L/2) = 0$. For $w = w' = 0$ and if $t \gg a^{-1}$, such that $L \gg \sqrt{\kappa/a}$, the solution is essentially time independent, and can be approximated as $p_\infty(x) \simeq \sqrt{(a/b)}\tanh(x/\lambda)$, with $\lambda = \sqrt{\kappa/a}$.

When the coupling of polarization to strain and contractility is turned on, various spatiotemporal patterns emerge as the active tension β' is varied. For small β', the stress patterns are qualitatively similar to Fig. 2(b) (with time-independent propulsion), and p asymptotically approaches p_∞ with initial oscillations near the midline [Figs. 4(a), 4(d)]. For intermediate β', a traveling stress pulse emerges in the layer and the location of stress maxima oscillate around the midline [Fig. 4(b)]. This is accompanied by large amplitude oscillations of net polarity that attenuate in time to generate a symmetric steady state polarization profile [Fig. 4(e)]. These traveling pulses persist even in the case $\beta = 0$. For even higher values of β', complex oscillatory patterns emerge in the monolayer stress and polarization [Figs. 4(c), 4(f)].

Discussions.—We have developed a simple yet rich dynamic model for an active spreading gel, based on a feedback between local strain and contractility. A local increase in length due to spreading promotes the assembly of active elements that in turn induce contraction. We propose that a finite turnover rate in the active contractile elements can yield an effective inertia and viscoelasticity in the gel that vanishes for infinitely fast turnover rates. This simple mechanochemical model allows us to capture the experimentally observed propagating stress waves during tissue expansion without invoking nonlinear elasticity [14]. These stress waves are characterized by strain rate wave fronts that initiate from the leading edge and periodically travel into and away from the midline of the monolayer. Our findings also elucidate that the effective material rigidity of the tissue undergoes sustained periods of stiffening and softening as the waves propagate. We emphasize that spreading is not crucial for wave propagation and that oscillations can also occur under confinement. In contrast to our model, Ref. [23] recently proposed that oscillatory modes in confined layers can also be generated by stochastic motion of cells. Experimental tests that inhibit myosin based contractility or cell directionality can help discriminate between these different models.

We thank Jeffrey Fredberg, James Butler, Jacob Notbohm, Michael Köpf, Sriram Ramaswamy and

Margaret Gardel for useful discussions. The work at Syracuse University was supported by the National Science Foundation (NSF) Grants No. DMR-1305184 and No. DGE-1068780. M. C. M. also acknowledges support from the Simons Foundation and from NSF Grant No. PHY11-25915 at the KITP of the University of California, Santa Barbara, and thanks KITP for its hospitality during completion of some of this work. S. B. gratefully acknowledges support from the Kadanoff-Rice fellowship through NSF Materials Research Science and Engineering Center at the University of Chicago.

*To whom correspondence may be addressed.
†shiladityab@uchicago.edu
‡mcmarche@syr.edu

[1] T. Mammoto and D. E. Ingber, Development (Cambridge, U.K.) **137**, 1407 (2010).
[2] R. Keller, Science **298**, 1950 (2002).
[3] G. Fenteany, P. A. Janmey, and T. P. Stossel, Curr. Biol. **10**, 831 (2000).
[4] T. Tsuji, S. Ibaragi, and G.-f. Hu, Cancer Res. **69**, 7135 (2009).
[5] C. J. Weijer, J. Cell Sci. **122**, 3215 (2009).
[6] M. L. Manning, R. A. Foty, M. S. Steinberg, and E.-M. Schoetz, Proc. Natl. Acad. Sci. U.S.A. **107**, 12517 (2010).
[7] A. F. Mertz, Y. Che, S. Banerjee, J. M. Goldstein, K. A. Rosowski, S. F. Revilla, C. M. Niessen, M. C. Marchetti, E. R. Dufresne, and V. Horsley, Proc. Natl. Acad. Sci. U.S.A. **110**, 842 (2013).
[8] X. Serra-Picamal, V. Conte, R. Vincent, E. Anon, D. T. Tambe, E. Bazellieres, J. P. Butler, J. J. Fredberg, and X. Trepat, Nat. Phys. **8**, 628 (2012).
[9] K. Kruse, J.-F. Joanny, F. Jülicher, J. Prost, and K. Sekimoto, Eur. Phys. J. E **16**, 5 (2005).
[10] J. S. Bois, F. Jülicher, and S. W. Grill, Phys. Rev. Lett. **106**, 028103 (2011).
[11] M. Marchetti, J. Joanny, S. Ramaswamy, T. Liverpool, J. Prost, M. Rao, and R. A. Simha, Rev. Mod. Phys. **85**, 1143 (2013).
[12] K. V. Kumar, J. S. Bois, F. Jülicher, and S. W. Grill, Phys. Rev. Lett. **112**, 208101 (2014).
[13] J. C. Arciero, Q. Mi, M. F. Branca, D. J. Hackam, and D. Swigon, Biophys. J. **100**, 535 (2011).
[14] M. H. Köpf and L. M. Pismen, Soft Matter **9**, 3727 (2013).
[15] S. Banerjee and M. C. Marchetti, Soft Matter **7**, 463 (2011).
[16] S. Banerjee, T. B. Liverpool, and M. C. Marchetti, Europhys. Lett. **96**, 58004 (2011).
[17] M. Radszuweit, S. Alonso, H. Engel, and M. Bär, Phys. Rev. Lett. **110**, 138102 (2013).
[18] P.-Y. Plaçais, M. Balland, T. Guérin, J.-F. Joanny, and P. Martin, Phys. Rev. Lett. **103**, 158102 (2009).
[19] K. Dierkes, A. Sumi, J. Solon, and G. Salbreux, Phys. Rev. Lett. **113**, 148102 (2014).
[20] J. H. Kim, X. Serra-Picamal, D. T. Tambe, E. H. Zhou, C. Y. Park, M. Sadati, J.-A. Park, R. Krishnan, B. Gweon, E. Millet *et al.*, Nat. Mater. **12**, 856 (2013).
[21] See Supplemental Material at http://link.aps.org/supplemental/10.1103/PhysRevLett.114.228101 for details on the model, linear stability analysis, and additional figures.
[22] X. Trepat, M. R. Wasserman, T. E. Angelini, E. Millet, D. A. Weitz, J. P. Butler, and J. J. Fredberg, Nat. Phys. **5**, 426 (2009).
[23] M. Deforet, V. Hakim, H. Yevick, G. Duclos, and P. Silberzan, Nat. Commun. **5** (2014).